

## EMISSION FROM LARGE-SCALE JETS IN QUASARS

YASUNOBU UCHIYAMA

*Department of High Energy Astrophysics, ISAS/JAXA,  
3-1-1 Yoshinodai, Sagamihara, Kanagawa, 229-8510, Japan  
E-mail: uchiyama@astro.isas.jaxa.jp*

We consider the emission processes in the large-scale jets of powerful quasars based on the results obtained with the VLA, *Spitzer*, *Hubble*, and *Chandra*. We show that two well-known jets, 3C 273 and PKS 1136–135, have two distinct spectral components on large-scales: (1) the low-energy (LE) synchrotron spectrum extending from radio to infrared, and (2) the high-energy (HE) component arising from optical and extending to X-rays. The X-ray emission in quasar jets is often attributed to inverse-Compton scattering of cosmic microwave background (CMB) photons by radio-emitting electrons in a highly relativistic jet. However, recent data prefer synchrotron radiation by a second distinct population as the origin of the HE component. We anticipate that optical polarimetry with *Hubble* will establish the synchrotron nature of the HE component. Gamma-ray observations with *GLAST* (renamed as the *Fermi* Gamma-ray Space Telescope), as well as future TeV observations, are expected to place important constraints on the jet models.

*Keywords:* galaxies: jets — quasars: individual(3C 273, PKS 1136–135) — radiation mechanisms: non-thermal

## 1. Introduction

The emission processes responsible for the spectral energy distributions (SEDs) of large-scale quasar jets, constructed using *Spitzer*, *HST* and *Chandra* data, are the subject of active debate.<sup>1</sup> The X-ray intensity relative to the radio synchrotron flux is generally too high to be explained by synchrotron-self-Compton.<sup>2</sup> The SED at radio, optical, and X-ray traces an inflected shape, which disfavors the interpretation of X-rays as due to synchrotron radiation from a single population of electrons.

Inverse-Compton (IC) scattering of CMB photons by high-energy electrons (with electron Lorentz factor of  $\gamma_e \sim 30$ ) in a highly relativistic jet with bulk Lorentz factor  $\Gamma \sim 10$  initially seemed an attractive way to explain the observed X-ray emission,<sup>3,4</sup> but this process is also not free of problems.<sup>5</sup> Finally, the X-rays may arise from synchrotron radiation from extremely energetic protons.<sup>6</sup> Determining which of these emission mechanisms produces the observed X-ray jets in powerful quasars is a strong motivation for more observations of radio-loud quasars, and has resulted in a rapid increase in the number of known X-ray jets.

In this work, we highlight new results based on the multiwavelength data from the VLA, *Hubble*, *Spitzer* and *Chandra*, aiming at identifying the radiation mechanisms operating in powerful quasar jets. The jets in the nearest quasar 3C 273 ( $z = 0.158$ ) and in the lobe-dominated quasar PKS 1136–135

( $z = 0.554$ ) are selected for our detailed analysis.

## 2. Quasar Jets in 3C 273 and PKS 1136–135

### 2.1. Image

Figure 1 (from Ref. 7) presents a three-color image of the large-scale jet in 3C 273 made with *Spitzer*, *HST*, and *Chandra* (with the VLA contours overlaid). The *Spitzer* photometry at  $3.6 \mu\text{m}$  is illustrated as a series of best-fitted PSFs of every knot to restore a resolution similar to the X-rays. The *HST* image represents an “UV excess” map emphasizing the near-ultraviolet light. The inner knots (A–B3) closer to the quasar core are bright in both the UV excess and X-rays, while the outer knots (C2–H3) are bright in the mid-infrared. Recent far UV imaging at 150 nm with *HST* indeed confirmed that the inner knots are bright in UV.<sup>9</sup>

In Fig. 1 we also present a three-color multifrequency image of the jet in quasar PKS 1136–135 (from Ref. 8). At the positions of optically bright knots A and B we depict a dot to indicate secure detections with *HST*.<sup>10</sup> The brightness patterns along the jet in various bands appear to be broadly similar to the 3C 273 jet. Like 3C 273, the jet knots can be divided up into two parts: the inner knots (A and B) and the outer knots (C, D, and E). The inner knots are bright in both the optical and X-rays, and as such they are high-energy dominated.

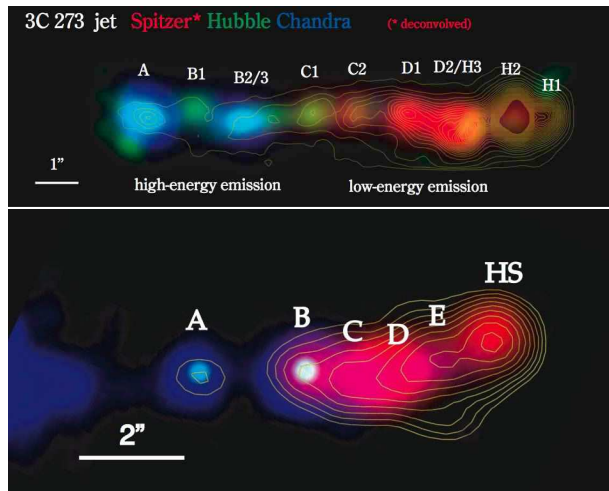


Fig. 1. (Top) *Spitzer-HST-Chandra* composite image of the jet in 3C 273 (Ref. 7): *Spitzer* “reconstructed”  $3.6 \mu\text{m}$  (red), *HST* “UV excess” (green), and *Chandra* 0.4–6 keV (blue). The *VLA* 2 cm radio contours are superposed on the image, with the strongest radio source H2 being truncated. (Bottom) Composite image of the jet in PKS 1136–135 (Ref. 8): *Spitzer* (red), *HST* (green dots on knots A and B), and *Chandra* (blue). The superposed contours are from the *VLA* 8.5 GHz. Knot A is closest to the quasar core in both cases.

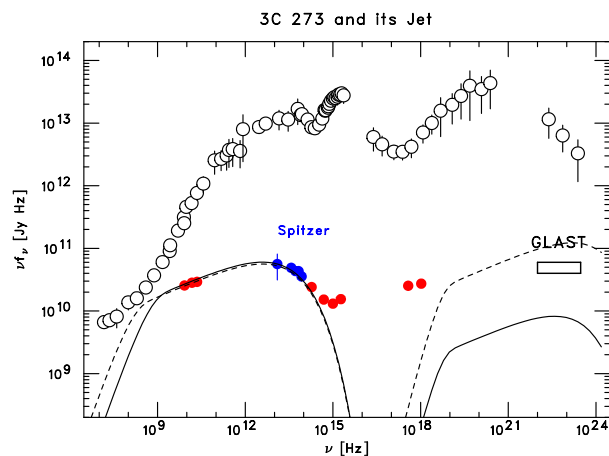


Fig. 2. Broadband SEDs of the core and large-scale jet in 3C 273. The quasar core (open circles) shows synchrotron and IC components of the small-scale jet as well as an accretion disk component in the optical.<sup>11</sup> The large-scale jet (accumulated over the entire length from knot A to H1) shows two components. The curves represent synchrotron radiation in the radio–infrared and its IC counterpart in gamma-rays: for a jet Doppler factor of  $\delta = 4$  (solid curves) and  $\delta = 8$  (dashed curves).

## 2.2. SED

In Fig. 2, the SEDs of both the quasar core and the jet in 3C 273 are shown. The fluxes of the quasar core, originated in a small-scale jet and an accretion disk of the central supermassive black hole, are described in Ref. 11. The jet SED is a “summed” spectrum for all the knots in Fig. 1 (Refs. 7,9,12). Here, we added new (unpublished) data points at 4.8, 8.0 and  $24 \mu\text{m}$  in the infrared using the *Spitzer* IRAC and MIPS. A very wide band from mid IR ( $24 \mu\text{m}$ ) to far UV ( $0.15 \mu\text{m}$ ) is covered with *HST* and *Spitzer*, revealing a spectral character of quasar jets with unprecedented details.

We compare SEDs of the large-scale jets in 3C 273 and PKS 1136–135 in Fig. 3. The two SEDs share common features. The optical and UV fluxes of the jet have a clear excess over the extrapolation from the infrared wavelengths, indicating that two spectral components cross over at optical wavelengths. We identify two spectral components as follows: (1) the low-energy (LE) synchrotron spectrum extending from radio to infrared with a spectral cutoff at  $\sim 5 \times 10^{13}$  Hz, and (2) the high-energy (HE) component arising in the optical and smoothly connecting to the X-ray flux. The two-component nature of the jet SED becomes more apparent if we construct knot-by-knot SEDs (see Refs. 7,9). Each SED shows the two components with varying relative strengths such that the low-energy part becomes more dominant with increasing distance from the quasar core. The position of the spectral cutoff of the LE component seems similar from one knot to another. Interestingly, in 3C 273, the spectral slopes of the HE component change from  $\alpha_{\text{HE}} \simeq 0.7$  (inner knots) to  $\alpha_{\text{HE}} \simeq 1.0$  (outer knots).

## 3. Discussion

### 3.1. LE component

Let us deduce some physical parameters of the LE spectral component, which is synchrotron radiation by relativistic electrons in the jet. The observed jet radiation is enhanced by Doppler beaming. (The Doppler factor is defined as  $\delta \equiv [\Gamma(1 - \beta \cos \theta)]^{-1}$  with  $\beta c$  the velocity of the jet,  $\Gamma = (1 - \beta^2)^{-1/2}$  the bulk Lorentz factor of the jet, and  $\theta$  the observing angle with respect to the jet direction.)

The LE synchrotron emission has a high-energy cutoff at  $\nu_c \simeq 5 \times 10^{13}$  Hz, presumably associated

with the maximum energy of the electron population. The maximum energy can be deduced as  $E_{\max} \sim 0.2 (B_{-4}\delta)^{-0.5}$  TeV, where  $B_{-4} = B/(0.1 \text{ mG})$  is the comoving magnetic field strength. The equipartition magnetic field is  $B\delta \sim 0.1 \text{ mG}$  for 3C 273 and  $B\delta \sim 0.7 \text{ mG}$  for PKS 1136–135.

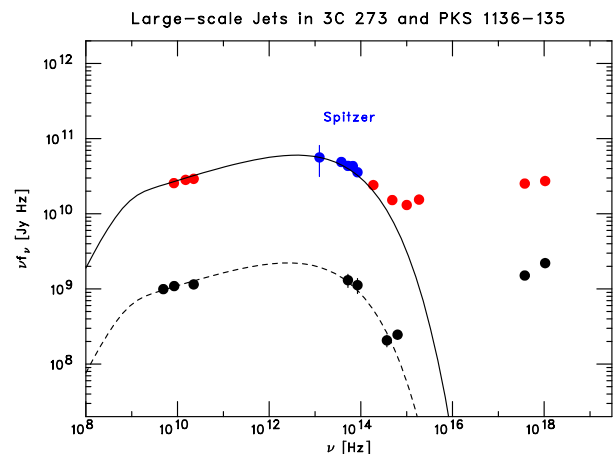


Fig. 3. SEDs of the large-scale jets in 3C 273 (taken from Fig. 2) and PKS 1136–135 (black filled circles: Ref. 8). The jet in PKS 1136–135 (fluxes extracted from knots A to E) has a two-component SED similar to 3C 273. The curves represent synchrotron radiation models.

By extrapolating VLA radio flux of knot H1/H2 in 3C 273 to lower frequencies (10–100 MHz), we found that a low energy “cutoff” or “break” should be present as well. Otherwise, the jet radio flux around  $\sim 100$  MHz exceeds even the total radio flux of 3C 273. It would be reasonable to assume that such a cutoff/break is common to all the knots. We adopt  $E_{\min} \sim 1000m_e c^2$  in Fig. 2 to introduce the low energy cutoff. Also, the observed synchrotron spectra from the radio to optical frequencies are likely to be formed in a “cooling regime”, and therefore a cooling break may appear in low-frequency radio bands.

Using the relation  $s_{LE} = 2\alpha_{LE}$ , where  $s_{LE}$  is acceleration index, the observed index of  $\alpha_{LE} \simeq 0.7$  is translated into the electron acceleration index of  $s_{LE} \simeq 1.4$ , close to the hardest possible index ( $s = 1.5$ ) in the nonlinear shock acceleration theory. Here we assumed particle acceleration taking place in each knot, where relativistic electrons are accumulated over a certain timescale of  $10^5$  to  $10^7$  yr. Assuming that the number of radio-emitting electrons is balanced by the number of cold protons in the jet, we estimated a jet kinetic power of  $L_{\text{kin}} \sim 5 \times 10^{44} \text{ erg s}^{-1}$

with  $\delta = \Gamma = 4$  and the equipartition magnetic field.

### 3.2. HE component: IC/CMB or synchrotron?

The beamed IC scenario<sup>3,4</sup> was initially considered to be an attractive explanation of the X-ray-dominated component of the SED for jet knots in radio-loud quasars, like 3C 273 (Ref. 13) and PKS 1136–135 (Refs. 10,14). We argued for a direct connection between the optical and X-ray fluxes.<sup>7</sup> The same mechanism should be responsible for the optical and X-ray emissions. If one adopts the beamed IC model for the X-rays, the energy distribution of electrons has to continue down to very low energies of  $E_{\min} \sim m_e c^2$  to account for the optical emission.

In the framework of the beamed IC radiation, it is interesting to note that the jet exhibits the evolution of multiwavelength emission along the jet as shown in Fig. 1. The increase of radio brightness is accompanied by the decrease of X-ray brightness towards downstream, which can be understood in terms of deceleration of the jet.<sup>10,14,15</sup> If the beamed IC scenario is correct, we are able to study the flow structure of the large-scale jets.

New results indicate, however, that the beamed IC scenario faces several difficulties. First, in the outer knots of the 3C 273 jet, the radio spectral index of  $\alpha_{LE} \simeq 0.7$  disagrees with the HE spectral index of  $\alpha_{HE} \simeq 1.0$  (see Refs. 7,12). Second, the parameters required in the beamed IC/CMB model are often too extreme. In the case of 3C 273, we obtained a Doppler factor of  $\delta = 30$  for knot A and a jet kinetic power of  $L_{\text{kin}} \simeq 1 \times 10^{48} \text{ erg s}^{-1}$ . The obtained Doppler factor seems too large for 3C 273, since relatively large contributions from the un-beamed components are observed in the core emission (see Fig. 2) and accretion-disk emission appears to be comparable to the jet emission in the X-ray regime.<sup>16</sup> In the case of PKS 1136–135, we obtained a Doppler factor of  $\delta = 19$ , which is also difficult to reconcile with the lobe-dominated nature of the quasar.

Instead of the beamed IC, synchrotron radiation by a second population of high-energy electrons may account for the HE component. Then the spectral index of the HE component,  $\alpha_{HE} \simeq 0.5$ – $1.0$  in 3C 273 and PKS 1136–135, corresponds to  $s_{HE} \simeq 1.0$ – $2.0$ . However,  $s_{HE} \simeq 1.0$  would be incompatible with diffusive shock acceleration theory. This brings into question the idea that the second electron population

is accelerated through diffusive shock acceleration. The second synchrotron component may instead be due to turbulent acceleration operating in the shear layers.<sup>17</sup> Unlike the shock acceleration, a hard spectrum,  $s < 1.5$ , can be expected to form in the case of turbulent acceleration (i.e., second-order Fermi acceleration). This scenario should be tested by future TeV observations (see below).

### 3.3. GLAST (Fermi-LAT) observations

As detailed in Ref. 18, GLAST measurements of the quasar jets will provide us with new information (or constraints) about the jet emission. The infrared-emitting electrons in a relativistic jet inevitably emit GeV  $\gamma$ -rays through an IC/CMB process (see Fig. 2). The total radiative output is dominated by the multi-GeV  $\gamma$ -rays and their predicted flux with  $\delta \sim 7$  exceeds the 1-yr sensitivity offered by the GLAST LAT in the case of 3C 273. Also, the observations of PKS 1136–135 with GLAST may be able to test the IC/CMB hypothesis, since the beamed IC model with  $\delta \sim 20$  predicts the observable GeV flux.<sup>8</sup> Note that steadiness and hard spectrum can distinguish the large-scale emission from the core emission.

Moreover, if the HE fluxes are due to synchrotron radiation by electrons, the UV/X-ray-emitting electrons in a relativistic jet produce IC-upscattered TeV  $\gamma$ -rays. This offers a potential diagnostic tool to distinguish the origin of the HE component.

### 3.4. HST polarimetry

Finally we emphasize that optical polarimetry can be an effective way of discriminating the radiation models responsible for the optical-to-X-ray emission of the jets. In the beamed IC interpretation, the optical and X-ray emission are due to Compton up-scattering off the amplified CMB by high-energy electrons of  $\gamma_e \sim 3$  (optical) and  $\gamma_e \sim 100$  (X-ray). Unlike in the case of synchrotron models, the X-rays are expected to be *unpolarized* and the optical light is nearly unpolarized at most a few percent of polarization (see Fig. 4). Precise polarization measurements in the optical can in principle verify (or discard) the beamed IC model. Unfortunately, there have been no useful polarization observations of quasar jets with *HST* so far. Only for 3C 273, early *HST* polarimetry

of the jet was done but with the pre-COSTAR FOC and low significances.<sup>19</sup> Recently, *HST* polarimetry of PKS 1136–135 has been approved (PI: Eric Perlman). New polarimetry of quasar jets on large-scales will provide important clues as to the origin of the HE component.

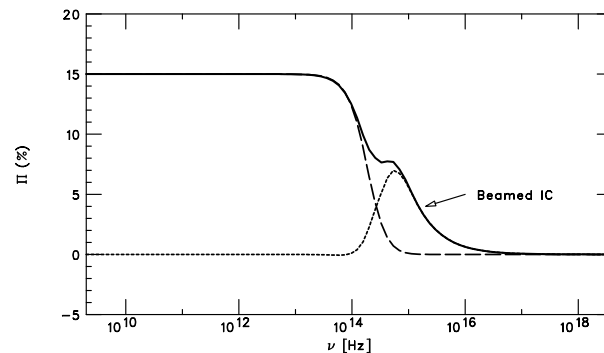


Fig. 4. The polarization degree in the synchrotron+IC model of knot A in the 3C 273 jet. The Doppler and Lorentz factor of a jet are  $\delta = \Gamma = 15$ . The minimum electron energy:  $E_{\min} = 2m_e c^2$ .

## References

- Harris, D. E., & Krawczynski, H. 2006, *ARA&A*, 44, 463
- Chartas, G., et al. 2000, *ApJ*, 542, 655
- Tavecchio, F., Maraschi, L., Sambruna, R. M., Urry, C. M. 2000, *ApJ*, 544, L23
- Celotti, A., Ghisellini, G., & Chiaberge, M. 2001, *MNRAS*, 321, L1
- Atoyan, A. M., & Dermer, C. D. 2004, *ApJ*, 613, 151
- Aharonian, F. A. 2002, *MNRAS*, 332, 215
- Uchiyama, Y., et al. 2006, *ApJ*, 648, 910
- Uchiyama, Y., et al. 2007, *ApJ*, 661, 719
- Jester, S., et al. 2007, *MNRAS*, 380, 828
- Sambruna, R. M., et al. 2006, *ApJ*, 641, 717
- Türlér, M., et al. 1999, *A&AS*, 134, 89
- Jester, S., Harris, D. E., Marshall, H. L., & Meisenheimer, K. 2006, *ApJ*, 648, 900
- Sambruna, R. M., et al. 2001, *ApJ*, 549, L161
- Tavecchio, F., et al. 2006, *ApJ*, 641, 732
- Georganopoulos, M., & Kazanas, D. 2004, *ApJ*, 604, L81
- Grandi, P., & Palumbo, G. G. C. 2004, *Science*, 306, 998
- Stawarz, L., & Ostrowski, M. 2002, *ApJ*, 578, 763
- Georganopoulos, M., Perlman, E., Kazanas, D., & McEnery, J. 2006, *ApJ*, 653, 5
- Thomson, R. C., Mackay, C. D., & Wright, A. E. 1993, *Nature*, 365, 133